Supporting information

Ultrathin Cu-MOF@δ-MnO$_2$ Nanosheets for Aqueous Electrolyte-based High-Voltage Electrochemical Capacitors

Electrochemical measurement

Traditional three-electrode system: The electrochemical performance was determined by a CHI 660E instrument in a traditional three-electrode system. A Hg/HgO electrode and platinum electrode were chosen as the reference and counter electrode, respectively. The electrolyte was a 1.0 M Na_2SO_4 aqueous solution. The working electrode materials were prepared by grinding the mixture of active materials, acetylene black, and PTFE with a weight ratio of 80:15:5, and coating the mixture on a 1 cm × 5 cm nickel foam. The additive was a certain amount of isopropyl alcohol when grinding, and the painted size was approximately 1 cm × 1 cm. In addition, the nickel foam with the coated activated materials was pressed to a thin foil at a pressure of 10.0 MPa.

Asymmetrical supercapacitor system: The electrochemical performance was conducted by a CHI 660E instrument in a traditional asymmetrical supercapacitor system. Aqueous electrochemical energy storage devices were assembled by employing the ultrathin Cu-MOF@δ-MnO$_2$ nanosheets as a positive electrode and activated carbon as a negative electrode. The electrolyte was a 1.0 M Na_2SO_4 aqueous solution. The activated carbon electrode was prepared by grinding a mixture of activated

carbon, acetylene black, and PTFE with a weight ratio of 80:15:5, and coating the mixture on a 1 cm × 5 cm nickel foam. The additive was a certain amount of isopropyl alcohol during grinding, and the painted size was approximately 1 cm × 1 cm. In addition, the nickel foam with the coat of activated materials was pressed to a thin foil at a pressure of 10.0 MPa.

Characterizations

The morphology of as-prepared samples was captured by a Supra 55 SEMat an acceleration voltage of 5.0 kV. The phase analysis of the samples was performed by a Bruker AXS D8 advanced XRD with Cu *Ka* radiation of 40 KV. Fourier transform infrared (FTIR) transmission spectra were obtained on a BRUKER-EQUINOX-55IR spectrophotometer. The surface chemical speciesof the samples were examined using a Perkin-Elmer PHI-5702 multifunctional XPS with Al15Ka radiation of 1486.6 eV as the excitation source. TEM images were observed on the JEM-2100 instrument microscopy at an acceleration voltage of 200 kV. Scanning transmissionelectron microscopy (STEM) images, HRTEM images, SAED images and EDS mappingwere captured on a Tecnai G2 F30 transmission electron microscopy at an accelerationvoltage of 300 kV. Nitrogen adsorption-desorptionmeasurements were performed on a Gemini VII 2390 analyzer at 77 K using the volumetric method. The specific

surface area was obtained from the N_2 adsorption-desorption isotherms and wascalculated by the BET method.All electrochemical performances were carried out by CHI 660E instrument.
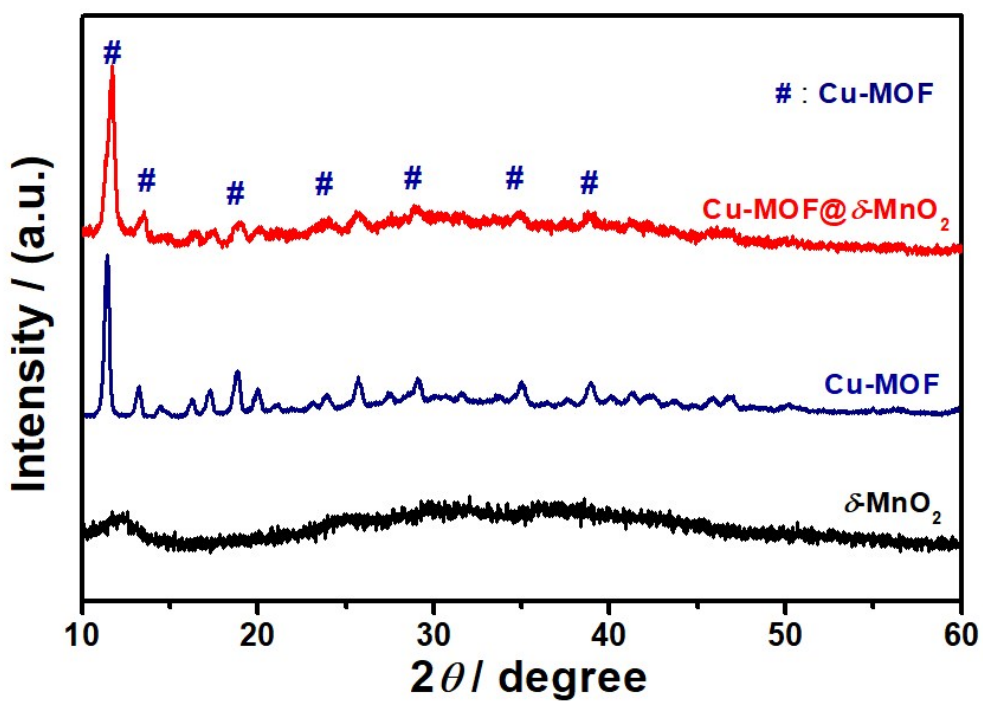
Figure S1. XRD patterns of Cu-MOF@δ-MnO$_2$, Cu-MOF and δ-MnO$_2$. ("#" marks show the obvious diffraction peaks of Cu-MOF)
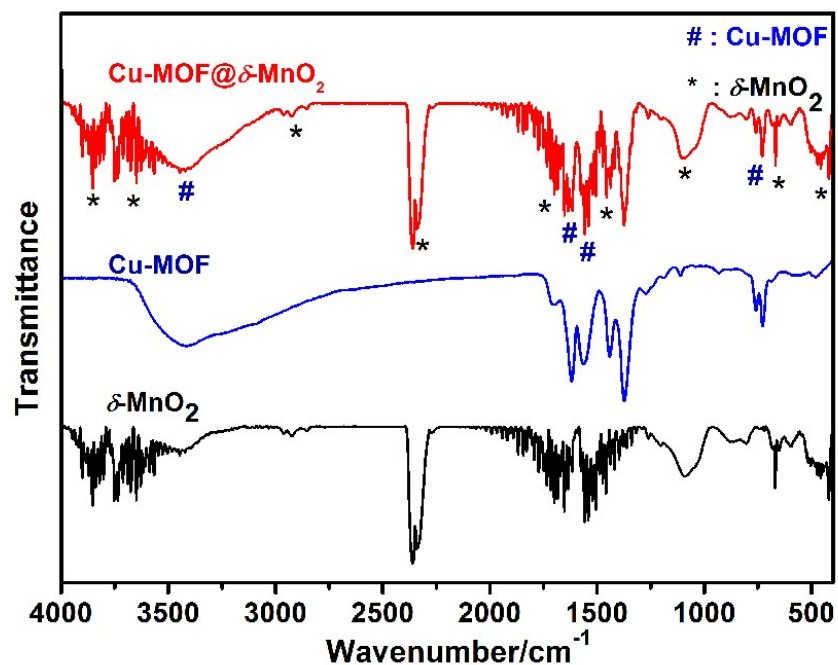
Figure S2. Fourier transform infrared spectroscopy (FT-IR) spectra of Cu-MOF@δ-MnO$_2$, Cu-MOF and δ-MnO$_2$.
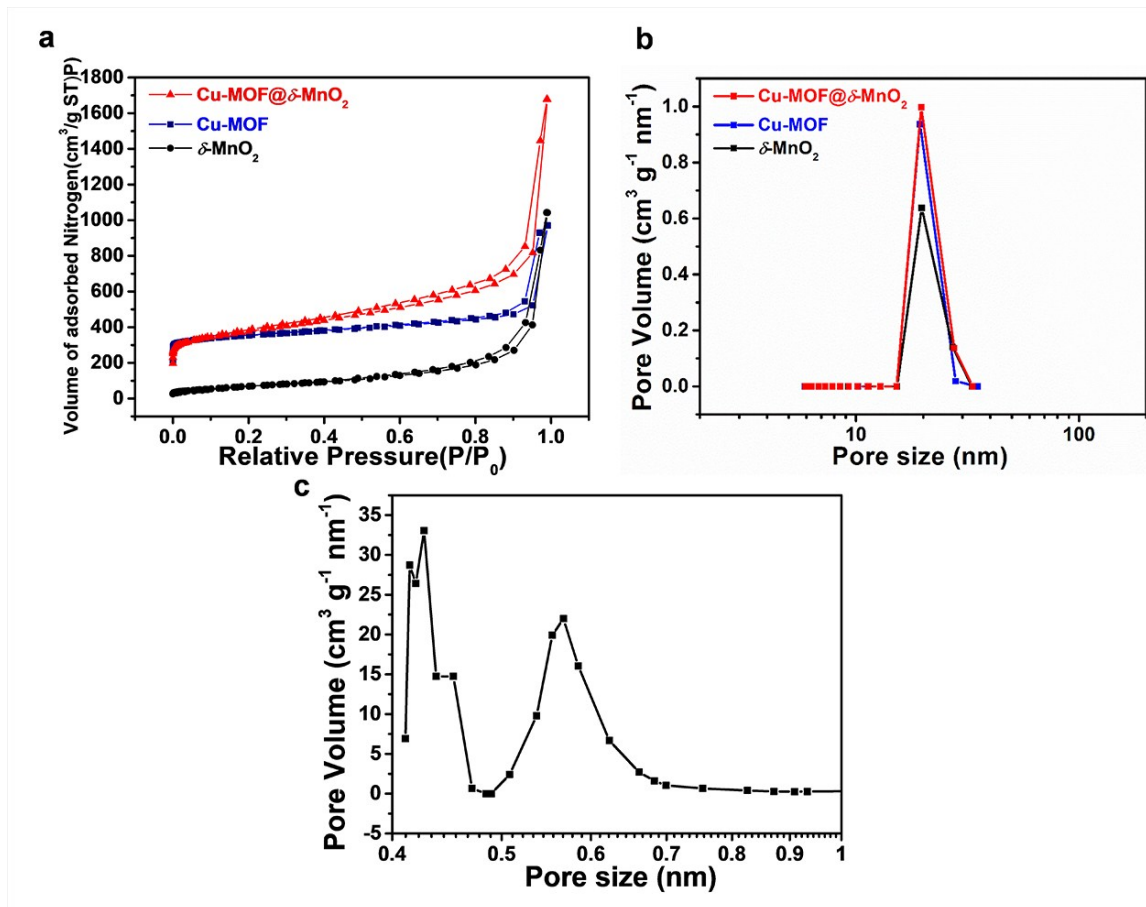
Figure S3. (a) Nitrogen adsorption-desorption isotherms, (b) pore size distribution curves of mesoporous for Cu-MOF@δ-MnO$_2$, Cu-MOF and δ-MnO$_2$, (c) pore size distribution curves of micropore for Cu-MOF@δ-MnO$_2$.
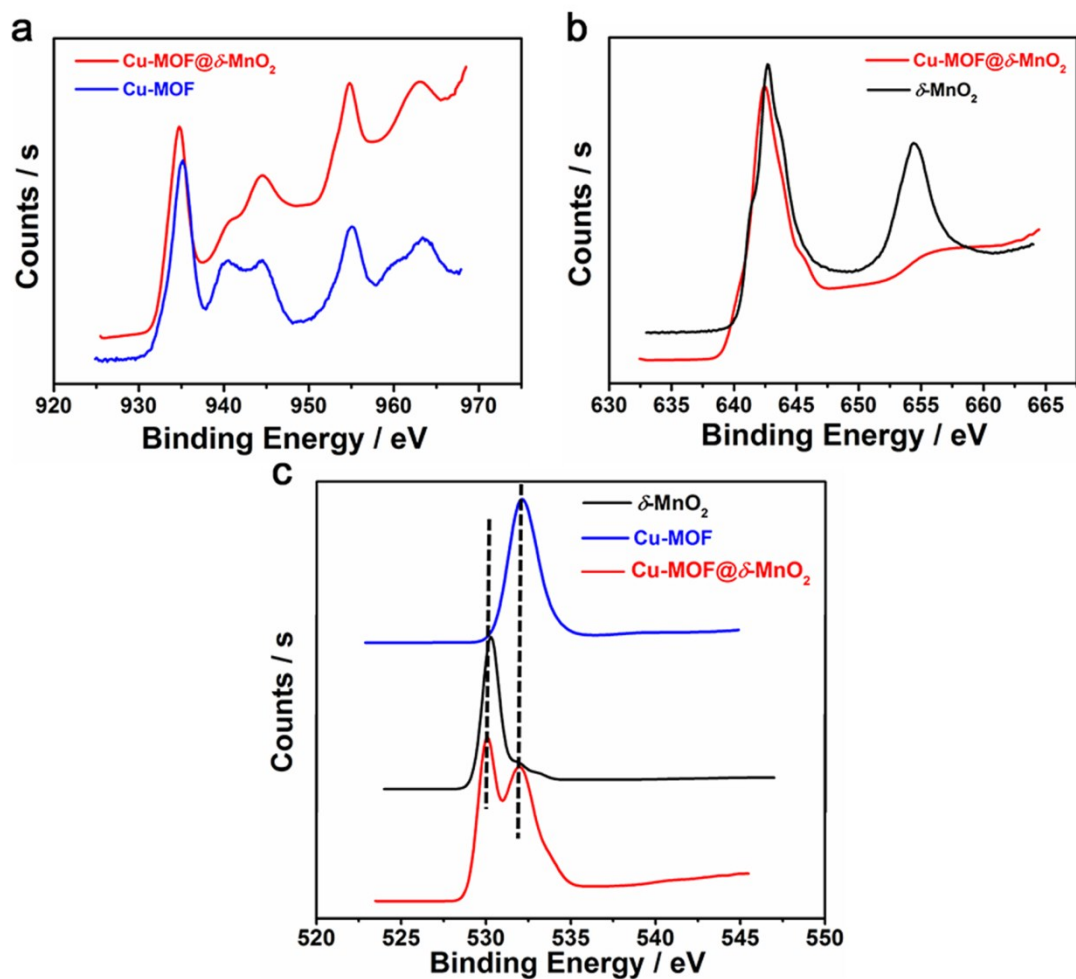
Figure S4. Comparisons of (a) Cu 2p, (b) Mn 2p and (c) O 1s XPS spectra of Cu-MOF, δ-MnO$_2$ and Cu-MOF@δ-MnO$_2$.
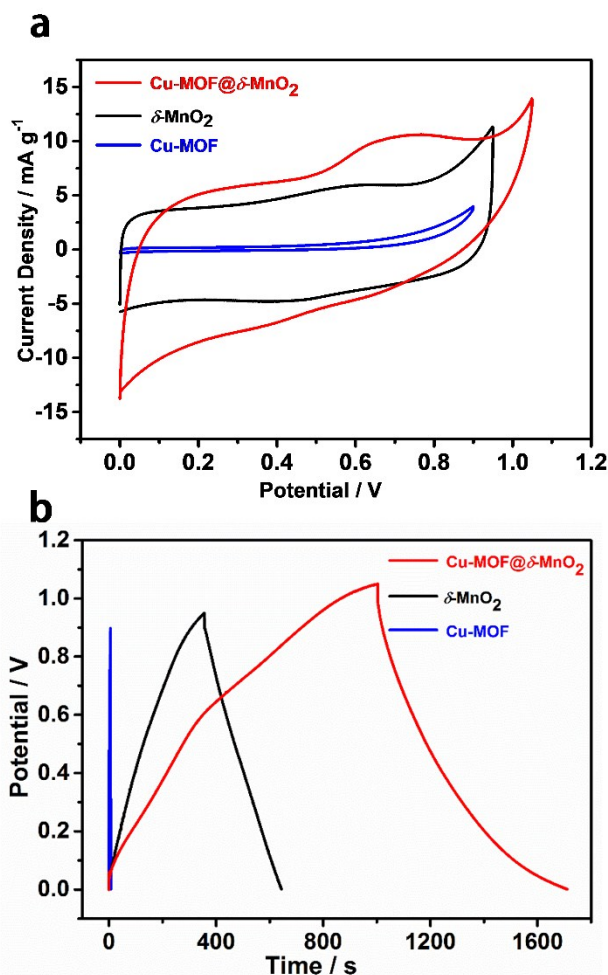
Figure S5. Comparison of Cu-MOF@*δ*-MnO₂ ultrathin nanosheets, Cu-MOF nanoparticles and *δ*-MnO₂ ultrathin nanosheets, (a) Cyclic voltammetry curves at different scan rates, (b) The galvanostatic charge-discharge curves at different current densities in 1.0 M Na₂SO₄ electrolyte with a three-electrode system.
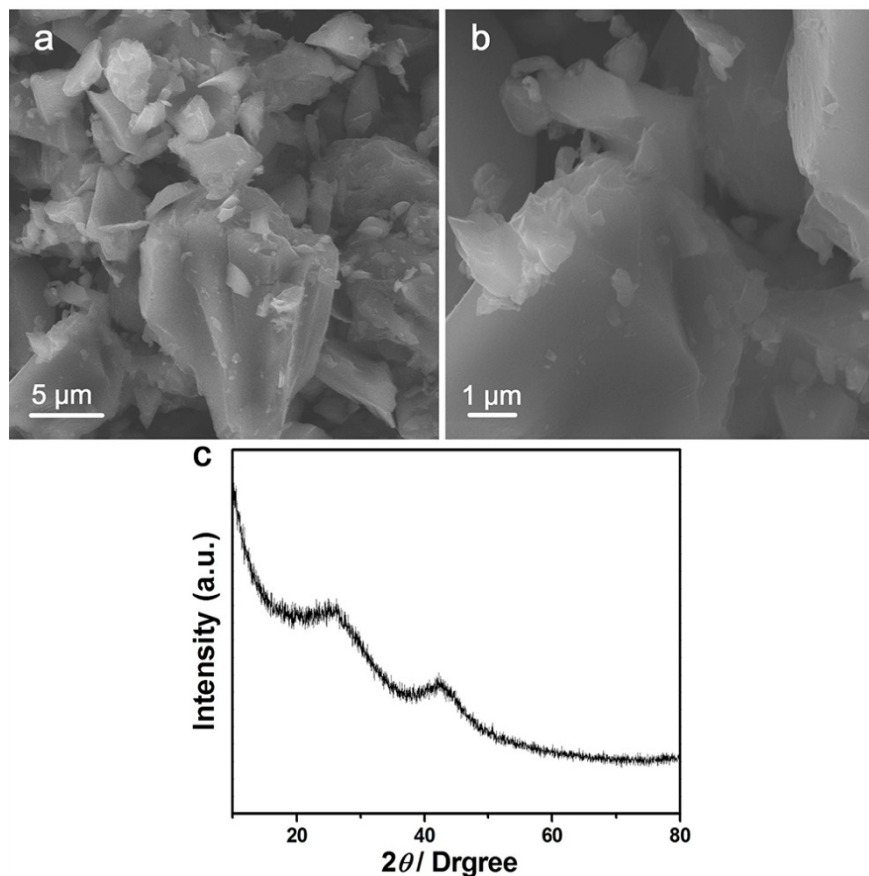
Figure S6. (a,b) Typical SEM images of activated carbon at different magnifications, (c) XRD pattern of activated carbon.
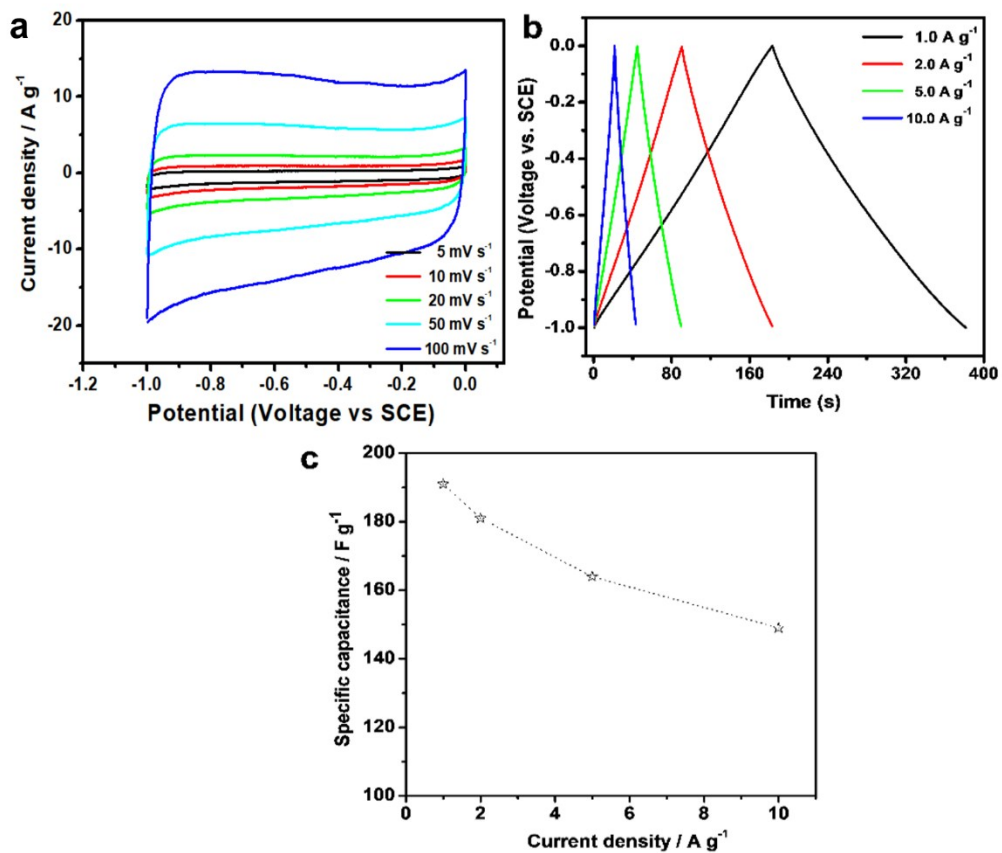
Figure S7. (a) Cyclic voltammetry curves of activated carbon electrode at different scan rates, (b) The galvanostatic charge-discharge curves of activated carbonelectrode at different current densities, (c) Specific capacitances of activated carbon electrode at different current densities in 1.0 M Na_2SO_4 electrolyte with a three-electrode system.
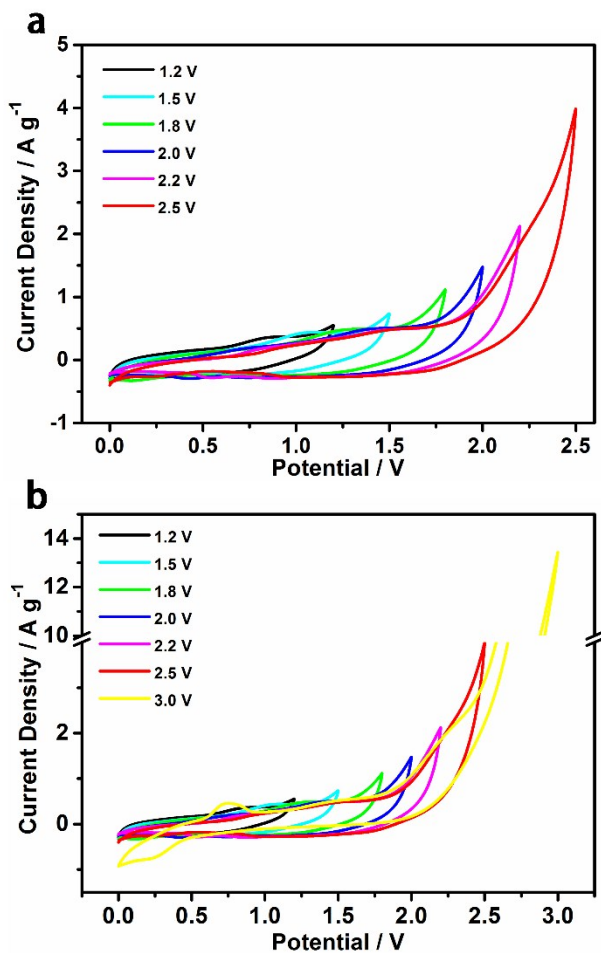
Figure S8. CV curves of the asymmetric supercapacitor under different potentials varying from 1.20-2.50 V (a), and 1.20-3.0 V (b) at 5 mV s^{-1}.
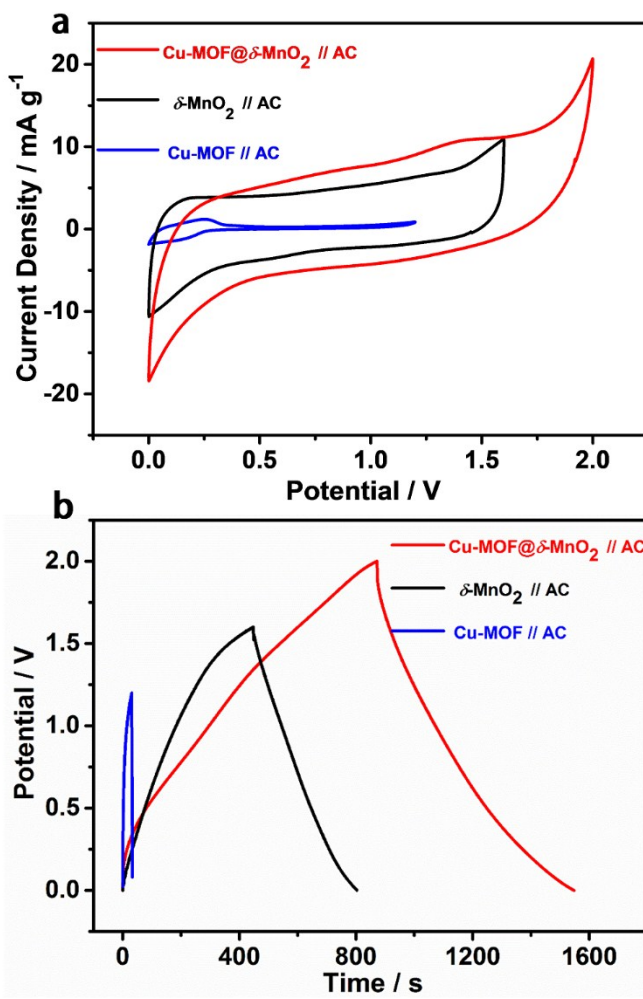
Figure S9. Comparison of Cu-MOF@δ-MnO$_2$ ultrathin nanosheets, Cu-MOF nanoparticles and δ-MnO$_2$ ultrathin nanosheets, (a) Cyclic voltammetry curves at different scan rates, and (b) The galvanostatic charge-discharge curves at different current densities in 1.0 M Na$_2$SO$_4$ electrolyte with an ASC devices.
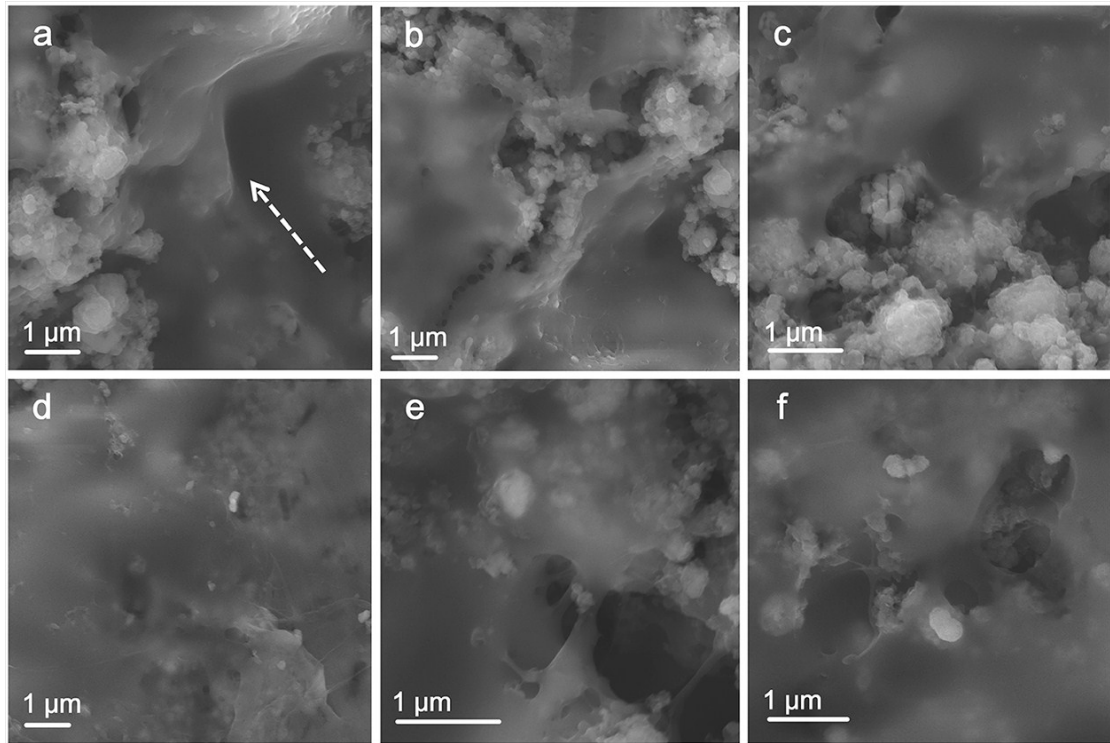
Figure S10. Typical SEM images of (a-c) Activated materials from the cycled composite electrode during the working process (0.5 cycle), and (d-f) Activated materials after the working process (1.0 cycle).
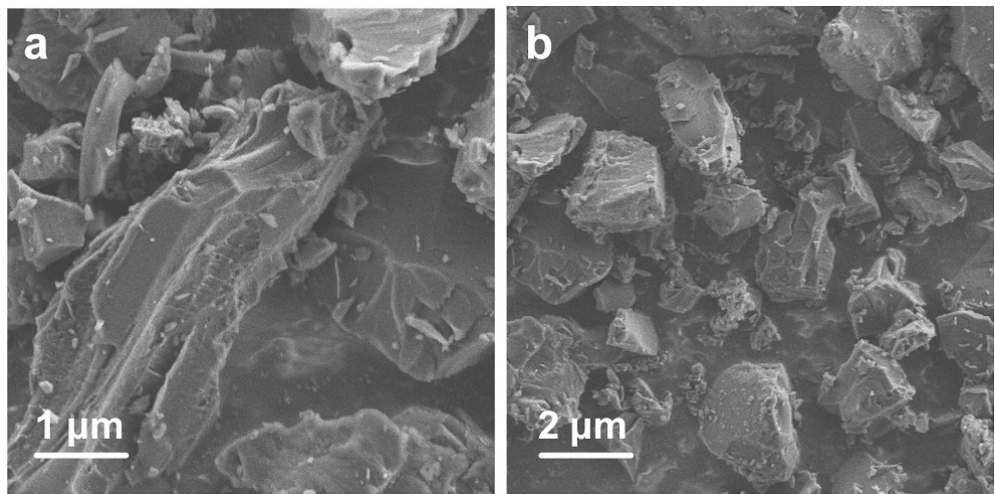
Figure S11. Typical SEM images of (a) Activated materials from the activated carbon electrode during the working process (0.5 cycle), and (b) after the working process (1.0 cycle).
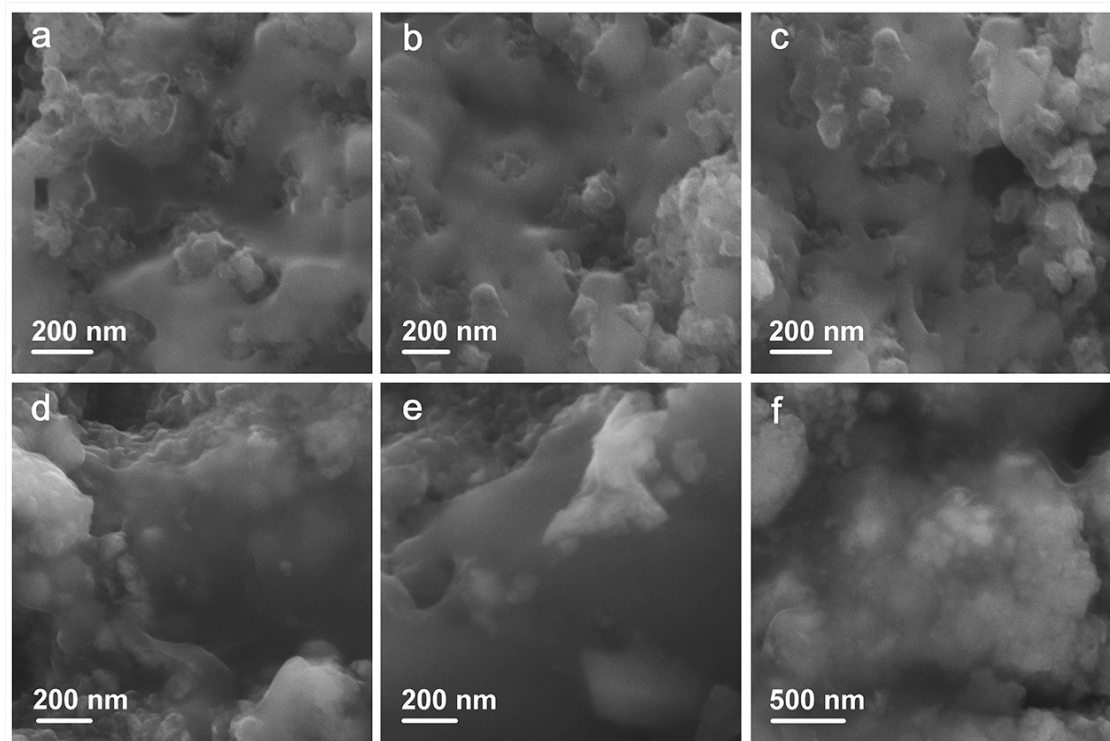
Figure S12. Typical SEM images of (a-c) Activated materials from the cycled composite electrode (without teflon) during the working process (0.5 cycle), and (d-f) Activated materials (without teflon) after the working process (1.0 cycle).
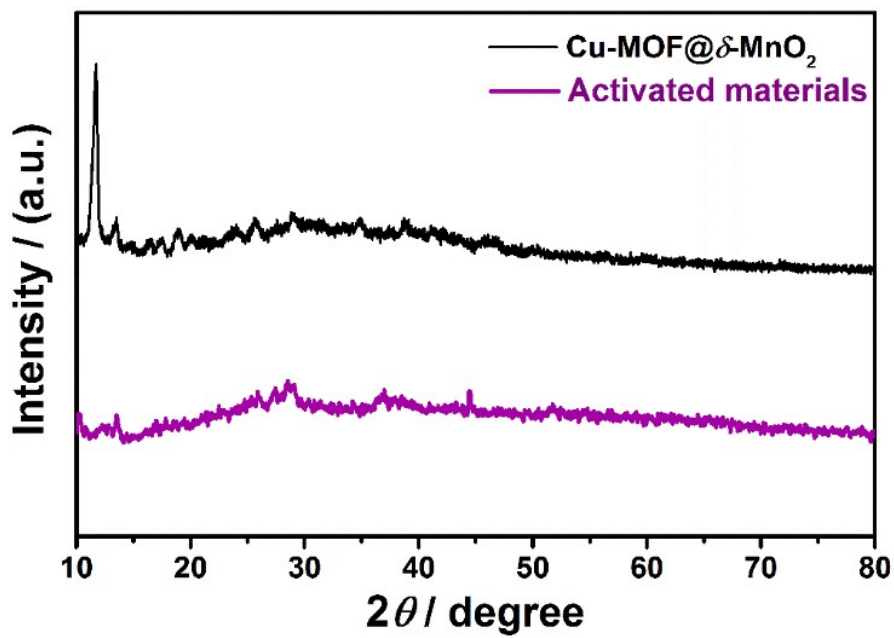
Figure S13. Comparison of XRD patterns of Cu-MOF@δ-MnO$_2$ and activated materials obtained after 25 cycles.
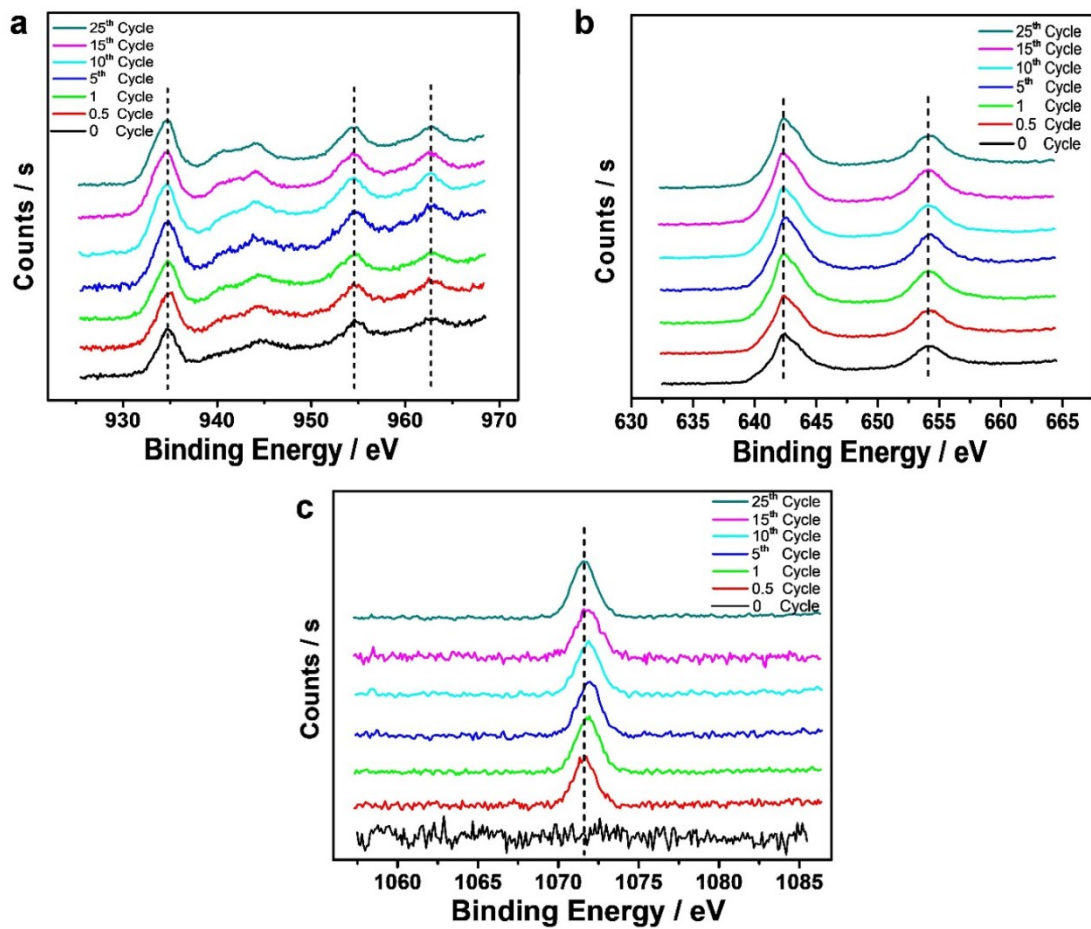
Figure S14. XPS spectra of the Cu-MOF@δ-MnO$_2$ ultrathin nanosheet samples during the working process (from 0 cycle to 25 the cycle), a) Cu 2p, b) Mn 2p and c) Na 1s.

Table 1. Comparisons with different MnO_2 based materials with a three-electrode system.

| Activated materials	Capacitance (F g^{-1})	E_{max}(Whkg^{-1})	P_{max}(W kg^{-1})	CR (%)/CN	Ref
MnO_2/GR gel/Ni foam	322/10 mV s^{-1}	-	-	45.7/200 mV s^{-1}	1
MnO_2/Sb-doped SnO_2	216/0.5 A g^{-1}	108	10625	91.5/5000	2
MnO_2/carbon microtube	617.6/1 A g^{-1}	-	-	80/1000	3
Diatomite/TiO_2/MnO_2	425/0.2 A g^{-1}	-	-	94.1/2000	4
MnO_2/CeO_2	274.3/0.5 A g^{-1}	-	-	93.9/1000	5
Carbon nanotube/MnO_2	145.6/5 mV s^{-1}	15.06	1498.5	98/1500	6
MnO_2/CNTs composite	149/0.2 A g^{-1}	-	-	90/5000	7
$NiMoO_4$/MnO_2	976/1 A g^{-1}	-	-	90.9/3000	8
MnO_2/N-graphene	453/2 A g^{-1}	-	-	114.4/4000	9
MnO_2 nanoparticles	280	-	-	92.31/500	10
$CoMoO_4$/MnO_2	1800/1A g^{-1}	-	-	96/30000	11
$NiCo_2S_4$@MnO_2	520.7/1 A g^{-1}	-	-	86.8/2000	12
Nickel-doped MnO_2	153.6/1 A g^{-1}	-	-	103/1000	13
$NiCo_2O_4$/MnO_2	13.9 F cm^{-2}	-	-	97.5/6000	14
Carbon nanofiber/MnO_2	257/5 mV s^{-1}	-	-	105/1000	15
MnO_2/$Ni_{0.75}Co_{0.25}O_y$	476.8/0.5 A g^{-1}	-	-	94.3/1000	16
MnO_2/carbon	202/0.25 A g^{-1}	-	-	~87/1000	17
MnO_2/ZnO	570.9 μF cm^{-2}	-	-	91.8/2000	18
MnO_2	197.3/1 A g^{-1}	-	-	94.6/1000	19
MnO_2/PPy	205/2 mV s^{-1}	-	-	96.5/400	20
grapheme/ MnO_2	319.8/0.2 A g^{-1}	31.5	1000	95/10000	21
GR/MnO_2 nanotube	290.6/1 A g^{-1}	-	-	90.7/3000	22
GR/MnO_2 nanoparticle	171.3/1 A g^{-1}	-	-	89.7/3000	22
GR/polyaniline/MnO_2	800.1/0.4 A g^{-1}	-	-	71/800	23
CuO/MnO_2	228	-	-	82.2/5000	24
This work	667/1 A g^{-1}			96.3/6000	

Table 2. Comparisons with other MnO_2 based materials with a two-electrode system.

Activated materials	Capacitance ($F g^{-1}$)	E_{max} ($Wh kg^{-1}$)	P_{max} ($W kg^{-1}$)	CR(%)/CN	Ref
MnO_2/GR gel/Ni foam	0.89/10 mV s^{-1}	0.72 mWh cm^{-3}	-	98.6/10000	1
$CoMoO_4$/MnO_2	152/1 A g^{-1}	54	8000	84/10000	11
$NiCo_2O_4$/MnO_2 //MoO_3@PPy	156.5/4 mA cm^{-2}	60.4	2400	88.2/10000	14
MnO_2/GR	267	18.64	12600	92/7000	25
MnO_2//Active carbon	315/5 mv s^{-1}	24.7	3500	92/6000	26
ε-MnO_2/$Ti_3C_2T_x$_Ar	212/1 A g^{-1}.	14.42	20000	88/10000	27
MnO_2/PANI/carbon	642/10 mV s^{-1}	39.9	642	88.1/1000	28
MnO_2 /GR-carbon	83.3/20 mV s^{-1}	84.3	5720	92/10000	29
Carbon/MnO_2//N-carbon	78.2/1 A g^{-1}	34.7	26800	91.2/2000	30
MnO_2/ carbon /GR	210/1 mA cm^{-2}	24	10000	95.7/1000	31
Bi_2O_3/CNF//MnO_2/CNF	25.2/1.5 mA cm^{-2}	11.3	3370	~85/4000	32
MnO_2/CNT//aerogel CNT	157.5 µF cm^{-1}/50 mVs^{-1}	46.59 nWh cm^{-1}	61.55 µW cm^{-1}	> 99/10000	33
NPG@MnO_2// CNTs/carbon	12 mF cm^{-2}	5.4 µWh cm^{-2}	2531 µW cm^{-2}	90/2000	34
H-MnO_2//RGO	449/0.75 mA cm^{-2}	0.25 mWh cm^{-3}	1.44 Wcm^{-3}	99/10000	35
MnO_2-ERGO//CNT-ERGO	69.4/ 0.5 A g^{-1}	31.8	9188.1	84.4/10000	36
H-TiO_2@MnO_2//H-TiO_2@C	139.6/1.1 A g^{-1}	59	45000	91.2/5000	37
GR/MnO_2 // GR/Ag	112.8/10 mV s^{-1}	50.8	90300	-	38
3DG/CNTs/MnO_2	343.1/ 2 mV s^{-1}	33.71	22727	95.3/1000	39
Co_3O_4/ MnO_2// carbon	353/5 A g^{-1}	~9.8	-	90.2/20000	40
MnO_2-PEDOT//AC ASC	503/1 mV s^{-1}	0.0018 Wh cm^{-3}	0.38 W cm^{-3}	99.5/4000	41
MnO_2/KCu_7S_4	533/1 mV s^{-1}	12.3	2020	85/6000	42
MnO_2/NiO@Ni	218/3 A g^{-1}	59.5	25350	75/10000	43
α-MnO_2 @ δ-MnO_2	276.9/1 A g^{-1}	78	21700	98.1/10000	44
α-MnO_2multiwalled carbon	99.7/1 mV s^{-1}	26.3	29400	77/20000	45
This work	340/1 A g^{-1}	79.1	20650	95/6000	

References

1   T. Zhai, F. Wang, M. Yu, S. Xie, C. Liang, C. Li, F. Xiao, R. Tang, Q. Wu, X. Lu and Y. Tong, *Nanoscale*, 2013, **5**, 6790.

2   S. Park, H.-W. Shim, C. W. Lee, H. J. Song, I. J. Park, J.-C. Kim, K. S. Hong and D.-W. Kim, *Nano Res.*, 2015, **8**, 990–1004.

3   X. Zhang, X. Meng, S. Gong, P. Li, L. Jin and Q. Cao, *Mater. Lett.*, 2016, **179**, 73–77.

4   X. L. Guo, M. Kuang, F. Li, X. Y. Liu, Y. X. Zhang, F. Dong and D. Losic, *Electrochim. Acta*, 2016, **190**, 159–167.

5   H. Zhang, J. Gu, J. Tong, Y. Hu, B. Guan, B. Hu, J. Zhao and C. Wang, *Chem. Eng. J.*, 2016, **286**, 139–149.

6   D. Ganguly, D. Pahari, N. S. Das, P. Howli, B. Das, D. Banerjee and K. K. Chattopadhyay, *J. Electroanal. Chem.*, 2016, **778**, 12–22.

7   P. Wu, S. Cheng, L. Yang, Z. Lin, X. Gui, X. Ou, J. Zhou, M. Yao, M. Wang, Y. Zhu and M. Liu, *ACS Appl. Mater. Interfaces*, 2016, **8**, 23721–23728.

8   H. Chen, L. Yu, J. M. Zhang and C. P. Liu, *Ceram. Int.*, 2016, **42**, 18058–18063.

9   H. R. Naderi, P. Norouzi and M. R. Ganjali, *Appl. Surf. Sci.*, 2016, **366**, 552–560.

10   S. R. Srither, A. Karthik, S. Arunmetha, D. Murugesan and V. Rajendran, *Mater. Chem. Phys.*, 2016, **183**, 375–382.

11   J. Wang, S. Liu, X. Zhang, X. Liu, X. Liu, N. Li, J. Zhao and Y. Li, *Electrochim. Acta*, 2016, **213**, 663–671.

12   H. Chen, X. L. Liu, J. M. Zhang, F. Dong and Y. X. Zhang, *Ceram. Int.*, 2016, **42**, 8909–8914.

13   Y. Yang, T. Liu, L. Zhang, S. Zhao, W. Zeng, S. Hussain, C. Deng, H. Pan and X. Peng, *J. Mater. Sci. Mater. Electron.*, 2016, **27**, 6202–6207.

14   S.-W. Zhang, B.-S. Yin, C. Liu, Z.-B. Wang and D.-M. Gu, *Chem. Eng. J.*, 2016, **312**, 296–305.

15   F. N. I. Sari, H.-M. Lin and J.-M. Ting, *Thin Solid Films*, 2016, **620**, 54–63.

16   N. Zhang, Y. Ding, J. Zhang, B. Fu, X. Zhang, X. Zheng and Y. Fang, *J. Alloys Compd.*, 2017, **694**, 1302–1308.

17   J. Lv, X. Yang, H. Zhou, L. Kang, Z. Lei and Z. H. Liu, *Mater. Res. Bull.*, 2016, **73**, 429–436.

18   X. Zhou and L. Ma, *Thin Solid Films*, 2015, **597**, 44–49.

19   S. Zhao, T. Liu, D. Hou, W. Zeng, B. Miao, S. Hussain, X. Peng and M. S. Javed, *Appl. Surf. Sci.*, 2015, **356**, 259–265.

20   L. Yuan, C. Wan and L. Zhao, *Int. J. Electrochem. Sci.*, 2015, **10**, 9456–9465.

21   J. Hao, Y. Zhong, Y. Liao, D. Shu, Z. Kang, X. Zou, C. He and S. Guo, *Electrochim. Acta*, 2015, **167**, 412–420.

22 C. Wang, F. Li, Y. Wang, H. Qu, X. Yi, Y. Lu, Y. Qiu, Z. Zou, B. Yu and Y. Luo, *J. Alloys Compd.*, 2015, **634**, 12–18.

23 K. Li, D. Guo, J. Chen, Y. Kong and H. Xue, *Synth. Met.*, 2015, **209**, 555–560.

24 Z. Zhang, C. Ma, M. Huang, F. Li, S. Zhu, C. Hua, L. Yu, H. Zheng, X. Hu and Y. Zhang, *J. Mater. Sci. Mater. Electron.*, 2015, **26**, 4212–4220.

25 L. Peng, X. Peng, B. Liu, C. Wu, Y. Xie and G. Yu, *Nano Lett.*, 2013, **13**, 2151–2157.

26 G. Wang, H. Xu, L. Lu, H. Zhao, Y. Tian and W. An, *J. Appl. Electrochem.*, 2016, **46**, 1091–1097.

27 R. B. Rakhi, B. Ahmed, D. Anjum and H. N. Alshareef, *ACS Appl. Mater. Interfaces*, 2016, **8**, 18806–18814.

28 Y. He, S. Du, H. Li, Q. Cheng, V. Pavlinek and P. Saha, *J. Solid State Electrochem.*, 2016, **20**, 1459–1467.

29 X. Ma, P. Kolla, Y. Zhao, A. L. Smirnova and H. Fong, *J. Power Sources*, 2016, **325**, 541–548.

30 Y. Luan, Y. Huang, L. Wang, M. Li, R. Wang and B. Jiang, *J. Electroanal. Chem.*, 2016, **763**, 90–96.

31 D. G. Lee and B. H. Kim, *Synth. Met.*, 2016, **219**, 115–123.

32 H. Xu, X. Hu, H. Yang, Y. Sun, C. Hu and Y. Huang, *Adv. Energy Mater.*, 2015, **5**, 1401882.

33 P. Xu, B. Wei, Z. Cao, J. Zheng, K. Gong, F. Li, J. Yu, Q. Li, W. Lu, J.-H. Byun, B.-S. Kim, Y. Yan and T.-W. Chou, *ACS Nano*, 2015, **9**, 6088–6096.

34 H. Xu, X. Hu, Y. Sun, H. Yang, X. Liu and Y. Huang, *Nano Res.*, 2015, **8**, 1148–1158.

35 T. Zhai, S. Xie, M. Yu, P. Fang, C. Liang, X. Lu and Y. Tong, *Nano Energy*, 2014, **8**, 255–263.

36 Z. Zhang, F. Xiao, L. Qian, J. Xiao, S. Wang and Y. Liu, *Adv. Energy Mater.*, 2014, **4**, 1400064.

37 X. Lu, M. Yu, G. Wang, T. Zhai, S. Xie, Y. Ling, Y. Tong and Y. Li, *Adv. Mater.*, 2013, **25**, 267–272.

38 Y. Shao, H. Wang, Q. Zhang and Y. Li, *J. Mater. Chem. C*, 2013, **1**, 1245–1251.

39 W. Chen, Y. He, X. Li, J. Zhou, Z. Zhang, C. Zhao, C. Gong, S. Li, X. Pan and E. Xie, *Nanoscale*, 2013, **5**, 11733.

40 X. Xia, D. Chao, Z. Fan, C. Guan, X. Cao, H. Zhang and H. J. Fan, *Nano Lett.*, 2014, **14**, 1651–1658.

41 Z. Su, C. Yang, C. Xu, H. Wu, Z. Zhang, T. Liu, C. Zhang, Q. Yang, B. Li and F. Kang, *J. Mater. Chem. A*, 2013, **1**, 12432.

42 S. Dai, Y. Xi, C. Hu, X. Yue, L. Cheng and G. Wang, *J. Power Sources*, 2015, **274**, 477–482.

43 S. Saha, S. Chhetri, P. Khanra, P. Samanta, H. Koo, N. C. Murmu and T. Kuila, *J. Energy Storage*, 2016, **6**, 22–31.

44 Z. Ma, G. Shao, Y. Fan, G. Wang, J. Song and D. Shen, *ACS Appl. Mater. Interfaces*, 2016, **8**, 9050–9058.

45 R. T. Vinny, K. Chaitra, K. Venkatesh, N. Nagaraju and N. Kathyayini, *J. Power Sources*, 2016, **309**, 212–220.